Robust Magnetic Properties of a Sublimable Single Molecule Magnet

Robust Magnetic Properties of a Sublimable Single Molecule Magnet

Evan Kiefl,[†] Matteo Mannini,[‡] Kevin Bernot,[¶] Xiaohui Yi,[¶] Alex Amato,[†] Tom Leviant,[§,†] Agnese Magnani,[∥] Thomas Prokscha,[†] Andreas Suter,[†] Roberta Sessoli,[‡] and Zaher Salman[*,†]

Laboratory for Muon Spin Spectroscopy, Paul Scherrer Institut, CH-5232 Villigen PSI, Switzerland, Department of Chemistry "Ugo Schiff", Universitï£¡ di Firenze & INSTM RU Firenze, via della Lastruccia 3-13, 50019 Sesto Fiorentino, Italy, INSA, ISCR, UMR 6226, F-35708 RENNES, 20 av.des buttes de Coï£¡smes CS70839, 35708 Rennes Cedex, France, Department of Physics, Technion - Israel Institute of Technology, Haifa 32000, Israel, and Department of Biotechnology, Chemistry and Pharmacy, Universitï£¡ di Siena & INSTM RU Siena, Via A. Moro, 2 53100 Siena, Italy

E-mail: zaher.salman@psi.ch

Abstract

The organization of single-molecule magnets (SMMs) on surfaces *via* thermal sublimation is a prerequisite for the development of future devices for spintronics exploiting

[*]To whom correspondence should be addressed

[†]Laboratory for Muon Spin Spectroscopy, Paul Scherrer Institut, CH-5232 Villigen PSI, Switzerland

[‡]Department of Chemistry "Ugo Schiff", Universitï£¡ di Firenze & INSTM RU Firenze, via della Lastruccia 3-13, 50019 Sesto Fiorentino, Italy

[¶]INSA, ISCR, UMR 6226, F-35708 RENNES, 20 av.des buttes de Coï£¡smes CS70839, 35708 Rennes Cedex, France

[§]Department of Physics, Technion - Israel Institute of Technology, Haifa 32000, Israel

[∥]Department of Biotechnology, Chemistry and Pharmacy, Universitï£¡ di Siena & INSTM RU Siena, Via A. Moro, 2 53100 Siena, Italy

the richness of properties offered by these magnetic molecules. However, a change in the SMM properties due to the interaction with specific surfaces is usually observed. Here we present a rare example of a SMM system which can be thermally sublimated on gold surfaces while maintaining its intact chemical structure and magnetic properties. Muon spin relaxation and ac susceptibility measurements are used to demonstrate that, unlike other SMMs, the magnetic properties of this system in thin films are very similar to those in the bulk, throughout the full volume of the film, including regions near the metal and vacuum interfaces. These results exhibit the robustness of chemical and magnetic properties of this complex and provide important clues for the development of nanostructures based on SMMs.

KEYWORDS: single molecule magnets · $[DyPyNO]_2$ · thin films · low energy muons spin relaxation · quantum tunneling of the magnetization

When looking at the future of information storage and processing, single-molecule magnets[1] (SMMs) offer promising ways of storing information in molecular units, a paradigm which approaches the information density limit. Recent advances in SMM synthesis are yielding high quality SMMs with large anisotropies that help preserve spin or magnetic states.[2] However, a prerequisite of any application is to better understand and control the magnetic properties of SMMs. Of particular interest is the behavior of these molecular nanomagnets at the nanoscale since their organization on solid surfaces (as monolayers or multilayer deposits) represents the likely architecture of any technological application.[3,4] There are only a few SMMs that allow nanostructure fabrication *via* wet chemistry approaches or physical deposition methods.[5] Depending on the chemical structure of the molecules, it is possible to transfer these fragile units to a surface, while maintaining almost unchanged magnetic properties, by chemical grafting from solution[6–8] or, even more rarely, by thermal treatment promoting their sublimation in vacuum without decomposition.[9–11] To date, the playground was essentially limited to two classes of molecular complexes: the propeller shaped tetra-Iron(III) cluster[12] and the Terbium(III) bisphthalocyaninato neutral complex ($TbPc_2$).[13] The latter is among the most investigated SMM systems due to the relatively simple deposi-

tion protocol.[9,14] Moreover, the presence of the lanthanide-based core offers the advantage of large magnetic moments and anisotropies, which result in large energy barriers that hinder thermally activated magnetic relaxation.[15–19] In fact, $TbPc_2$ based devices have been attracting considerable attention recently.[20,21] However, this system exhibits strong alteration of its magnetic properties due to its interaction with the substrates and changes in the molecular packing in films.[22–24] Therefore, the search for alternative SMM candidates, which maintain their bulk properties even in nanostructures is highly relevant and desirable.

Recently, some of us synthesized a Dy based dimer, $[Dy(hfac)_3(PyNO)]_2$ with hfac = hexafluoroacetylacetonate and PyNO is pyridine-N-oxide (Fig.1(a)). Hereafter, we refer to this compound as $[DyPyNO]_2$. This SMM consists of two Dy ions with an intramolecular Dy-Dy distance of 3.78(1)Å and a shortest crystalline intermolecular Dy-Dy distance of 9.84(8)Å[25] - a geometry that minimizes intermolecular dipolar interaction but allows a weak antiferromagnetic coupling between the intramolecular Dy moments, which becomes important only below $\sim$ 20 K.[25] At higher temperatures the spin dynamics are governed by isolated Dy single ion properties rather than the Dy-Dy interactions.[25] Each Dy moment has a doubly degenerate ground spin state $J_z = \pm 15/2$ that is well separated from the first excited state ($J_z = \pm 13/2$) by $\sim$ 167 K.[25] Therefore, magnetic relaxation at low temperatures is primarily due to spin fluctuations within the doubly degenerate ground state.

Successful deposition of the pristine $[DyPyNO]_2$ molecular system on top of a gold surface is demonstrated here by using X-ray photoelectron spectroscopy (XPS), time of flight secondary ion mass spectrometry (ToF-SIMS), and X-ray diffraction measurements (XRD). The magnetic properties, and in particular the evolution of spin dynamics of $[DyPyNO]_2$ as a function of temperature, was measured using muon spin relaxation (μSR). We find that these are virtually identical in bulk powder and a sublimated thin film, confirming that the magnetic properties of this system remain unaltered. While this may seem like a common occurrence, $[DyPyNO]_2$ is the first SMM to exhibit this behavior over the full temperature range.

Results and Discussion

Bulk powder samples of $[DyPyNO]_2$ were prepared as described elsewhere[25] and used to study the bulk properties of the complex. Thin film samples were fabricated using a home-made molecular evaporator chamber (see Methods). For XPS, ToF-SIMS, XRD and μSR measurements we used a film deposited on polycrystalline-gold ($\sim$ 100 nm) coated mica substrate. The thickness of this films was estimated to be $\sim$ 200 nm by parallel evaporation on glass and using AFM scratching measurements. The roughness of the film was estimated using AFM measurements to be $\sim$ 20 nm. Example topographs and details of the AFM characterization are available in the supporting information (SI). Furthermore, XRD investigations evidence the absence of a regular crystalline structure in the molecular film indicating an amorphous or highly disordered packing of the $[DyPyNO]_2$ units (see SI).

The magnetic properties of the $[DyPyNO]_2$ powder and film (1.5 mg of $[DyPyNO]_2$ film evaporated on 3.0 mg of Teflon tape) samples were studied using alternating current (ac) susceptibility. Measurements in zero static field, between 2 and 15K, and from 10 Hz to 10 kHz were obtained using a Quantum Design physical properties measurements system (PPMS). A more detailed investigation of the magnetic properties was performed using conventional muon spin relaxation (μSR)[26] on the bulk sample and low energy μSR (LE-μSR)[27,28] on the thin film (see Methods).

Stability upon sublimation of polynuclear molecular complexes is far from trivial. In fact, fragmentation of molecules due to the partial decomposition of the molecular architectures during deposition is well documented.[9,29–31] In the $[DyPyNO]_2$ case, XPS and ToF-SIMS characterizations of thick film deposits exclude such fragmentation problems. A semi-quantitative analysis of the Dy*4d*, C*1s*, N*1s*, O*1s*, and F*1s* regions (see Table in Fig. 1(b)) gives a good agreement with the expected composition of an intact molecular system. A careful analysis of the regions of interest (see SI) evidences that the spectral features of the system are fully maintained after the deposition. As expected, the Dy*4d* zone shows a complex spectrum due to *4d-4f* interactions, with the fine structure and main peak centered

(a)

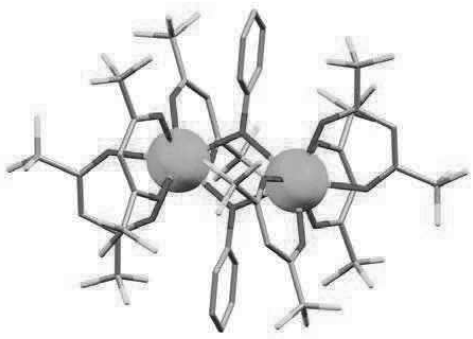

(b)

	C*1s*	Dy*4d*	F*1s*	N*1s*	O*1s*
theor.	42.6%	2.1%	38.3%	2.1%	14.9%
film	39.5%	2.6%	41.3%	2.2%	14.3%

	CF_3	CO	CN C(C=O)	CC	NO	CO
theor.	30.0%	30.0%	25.0%	15.0%	14%	86%
film	31.2%	29.6%	28.7%	10.5%	11%	89%

Figure 1: (a) Molecular structure of $[DyPyNO]_2$, color code: cyan spheres are Dy atoms while red, grey and green sticks are O, C, and F atoms, respectively. H atoms are omitted for clarity. (b) XPS semi-quantitative analysis of the sublimated film compared to the theoretical values. (c) ToF-SIMS characterization of pristine bulk material (blue) and the sublimated $[DyPyNO]_2$ film on Au (red). The low mass region (300-1000 m/z), high mass region (1000-1800) and two detailed regions are presented, the latter showing the corresponding theoretical isotopic distribution (see Table 1S in SI for the complete assignation list). Results of ac susceptibility measurements on (d) bulk powder $[DyPyNO]_2$ and (e) films grown on Teflon. (f) The relaxation time of the magnetization, τ_M, as a function of inverse temperature.

at 157 eV, perfectly in line with a $Dy^{(III)}$ system.[32,33] More interestingly the C*1s* spectrum shows a fine structure where the contributions of the different carbon atoms are clearly identified according to previous reports on similar systems.[34,35] At high beam energy (BE), the peak centered at 291.8 eV is attributed to the fluorinated carbon (CF_3) atoms and the ketonic carbon atoms (C=O) at 286.7 eV are easily distinguished. Other contributions at lower BEs, which can be extracted with the support of a deconvolution analysis, are in good agreement with the theoretical values expected for the intact system (see Table in Fig.1(b)). A similar treatment on the O*1s* zone reveals the presence of two distinct contributions; one from the pyridine-N-oxide and the other from ketonic oxygen. A direct comparison between ToF-SIMS of the pristine bulk material and the sublimated $[DyPyNO]_2$ film leads to identical mass spectra, as shown in Fig. 1(c). Although the molecular peak (1759.86 m/z) cannot be resolved, several lower mass signals confirm that the evaporation does not alter the chemical structure. This is clearly seen by the identical fragmentation patterns (see Table 1S in SI for the complete assignation list). The most intense peak is found in both bulk and film at 768 m/z and is attributed to the $[Dy+(hfac)_2+(PyNO)_2]^+$ ion. This peak features an isotropic distribution pattern that is fully in line with the simulated spectrum. Similarly, other relevant signals at higher m/z can be found, in particular, we mention the $[M\text{-}(hfac)]^+$ signal detected at 1550 m/z whose pattern agrees with the theoretical one.

The ac susceptibility measurements on the evaporated film (Fig. 1(e)) reveal a very similar behavior to that observed in bulk (Fig. 1(d)). The presence of peaks in the imaginary component of the susceptibility, χ", which shifts with decreasing temperature is indicative of superparamagnetic behavior. In agreement with previous reports on bulk,[25] the film features a thermally activated regime at high temperature while at lower temperature the contribution from quantum tunnelling becomes relevant. The extracted relaxation time of the magnetization is shown in Fig. 1(f), varying over many orders of magnitude within the measured temperature range ($2 - 15$ K). While these measurements show a clear similarity between the magnetic properties of the bulk and film (averaged over the full volume), they cannot

exclude variations as a function of depth, *e.g.* near the free surface of the $[DyPyNO]_2$/Au interface. We will revisit this aspect in our discussion of the LE-μSR measurements below.

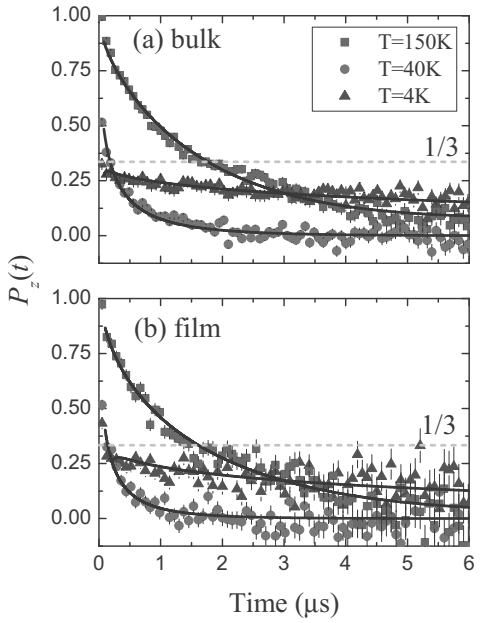

Figure 2: Muon-spin polarization as a function of time measured in (a) the bulk powder and (b) the thin film samples. The measurements are all in zero applied magnetic field. The solid lines are fits as described in the text. The dashed lines mark 1/3 polarization.

μSR measurements in zero applied magnetic field (ZF) were performed on bulk powder sample and a thin film grown on Au. Example muon-spin relaxation curves are presented in Fig. 2. At 4 K in the bulk $[DyPyNO]_2$ sample, approximately 2/3 of the muon-spin polarization ($P_z(t)$) undergoes extremely rapid depolarization, whereupon the remaining 1/3 tail slowly relaxes to zero (Fig. 2(a)). The behaviour in the thin-film displays a striking similarity to that observed in bulk, as seen in Fig. 2(b). This is evidence that the implanted muons experience a large, and randomly oriented, quasi-static internal field.[23] In such a case, the polarization of the ensemble of muons projected onto the local static field direction averages to 1/3 of the full polarization, while 2/3 is perpendicular to it. The 1/3 component may experience slow relaxation only due to a dynamic component in the local field, while the remaining 2/3 component undergoes incoherent precession and depolarizes at a rate which is determined by the width of the static field distribution. As the temperature is increased,

the depolarization rate decreases and no distinction between the two relaxing components is seen. Instead, a single exponential-like depolarization is observed.

Due to the broad distribution of local static magnetic fields at low T, the fast 2/3 component of $P_z(t)$ is at the limit of the timing resolution in a conventional μSR experiment. LE-μSR has even a lower timing resolution and hence this fast component cannot be resolved in the thin-film measurements. Therefore, we first analyze the bulk (fully resolved) results. Then, a comparison will be made between the thin-film and bulk sample using a more approximate method. Following the analysis method used in similar systems[23,36] we fit $P_z(t)$ in the bulk sample to a static Kubo-Toyabe function multiplied by an appropriate exponential-like relaxation,

$$P_z(t) = \left[\frac{1}{3} + \frac{2}{3}(1 - \Delta t - \sigma^2 t^2)e^{-\Delta t - \frac{\sigma^2 t^2}{2}}\right] e^{-\sqrt{\lambda t}}, \quad (1)$$

where Δ/γ ($\gamma = 2\pi \times 135.5$ MHz/T is the muon gyromagnetic ratio) is the Lorenzian width of static magnetic fields distribution due to the moments of the SMMs, σ/γ is the Gaussian width of the static fields distribution due to (primarily F and H) nuclear moments,[37] and λ is the relaxation rate due to the dynamic component of the local field. The square root exponential relaxation reflects the averaging of the relaxation behavior of muons stopping in many nonequivalent sites.[23,36,38,39] The results of the fits are shown in Figs. 3(a) and (b), where σ is assumed to be a common and temperature independent parameter. From the fits we find $\sigma = 0.129(6)$ MHz or correspondingly, a nuclear dipolar field distribution width of 0.152(7) mT.

Similar to other SMMs studied using μSR, Δ is zero at high temperatures with a large upturn as the temperature is decreased and saturation in the low temperature regime, at a value of 61(4) MHz (Fig. 3(a)), which translates to a width of 72(5) mT. In Fig. 3(b), λ is small at higher temperatures, increases to a maximum value as the temperature is decreased, then decreases to small values in the low temperature regime and becomes almost

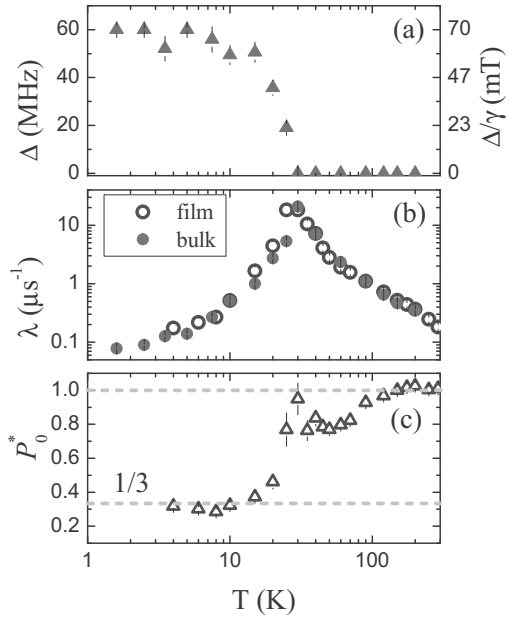

Figure 3: (a) The temperature dependence of Δ extracted from the bulk sample data. (b) The temperature dependence of λ for bulk (full symbols) and thin-film (open symbols). (c) The values of P_0^* as a function of temperature obtained from fitting the thin-film data to Eq. (2), with the dashed lines indicating full and 1/3 polarization.

temperature independent. Note that the onset of non-zero Δ and the peak of λ occur at the same temperature, a behavior typical of SMMs.[23,36,40,41]

We now turn to the discussion of the thin-film results and comparison with bulk. As we mentioned above, analysis of the thin-film data using Eq. (1) is not possible and may lead to incorrect results given the lower time resolution of LE-μSR. Instead, we use a very simple approximation of Eq. (1). Since at high temperature ($\Delta \longrightarrow 0$), Eq. 1 can be written as,

$$P_z(t) = P_0^* \left[\frac{1}{3} + \frac{2}{3}(1-\sigma^2 t^2)e^{-\frac{\sigma^2 t^2}{2}}\right] e^{-\sqrt{\lambda t}}, \qquad (2)$$

with $P_0^* \approx 1$. However, this approximation clearly does not agree with the low temperature behaviour, where we effectively cannot measure $P_z(t)$ at early times. To overcome this difficulty, we fit $P_z(t)$ starting only from $t = 0.05$ μs (to avoid distortions in $P_z(t)$ due to the limited time resolution) and fixing σ to the value obtained from bulk while allowing P_0^* to vary as a function of temperature to account for the almost immediate loss of polarization

at early times, *i.e.* when Δ is large. This analysis procedure enables a more quantitative comparison between film and bulk data. The results of this fit are presented in Figs. 3(b) and (c). We find that P_0^* goes from 1 at high temperature to 1/3 at low temperature, as expected when going from a regime where the local fields are fluctuating to a regime where they are quasi-static. Moreover, we find that the values of λ in both bulk and film exhibit excellent agreement over the whole temperature range. This is clear evidence that the fluctuations of the local fields, and thus the molecular spin dynamics, are the same in bulk and film.

Further, we performed LE-μSR measurements at different implantation depths in the $[DyPyNO]_2$/Au film. However, no depth dependence in λ or P_0^* was observed between 40 and 200 nm (see Fig. 2S in SI), clearly indicating that the molecular spin dynamics are not altered near the free surface or the $[DyPyNO]_2$/Au interface. This is in contrast to the case of $TbPc_2$ where the spin dynamics change dramatically with depth, in particular near the Au/$TbPc_2$ interface.[23] The lack of depth dependence can be attributed to the robustness of the $[DyPyNO]_2$ molecules even after evaporation and thin film deposition. It is important to point out here that the depth resolution of LE-μSR can detect variation on a scale of $\sim$ 10 nm, and therefore, our measurements cannot rule out changes in the magnetic properties of a few monolayers of $[DyPyNO]_2$, *e.g.* near interfaces. Note, however, the current investigation of thick films is a prerequisite for establishing the possibility of future studies of (sub-)monolayers of $[DyPyNO]_2$ deposited by the same evaporation technique.

In interpreting the results for the bulk sample presented in Fig. 3, the parameters Δ and λ provide a complete characterization of the spin dynamics. The most striking feature in the temperature dependence of λ is the abrupt peak observed near $\sim$ 30 K. At this temperature the local magnetic fields (sensed by the muon) go from fast dynamics at high T to quasi-static at low T. Since these fields originate from dipolar fields of the SMMs, they reflect the $[DyPyNO]_2$ spins dynamics. The small λ value and $\Delta \sim 0$ at high T are indicative of the fast spin fluctuations. As the temperature is decreased, the fluctuations slow down and λ increases gradually. At $\sim$ 30 K the fluctuations are slow enough that the dipolar

fields appear quasi-static for the muons; at this point Δ increases sharply while the dynamic contribution to the muon spin relaxation, λ, decreases as the fluctuations slow down further. The terms quasi-static and dynamic are relative to the ratio ν/Δ, where ν is the fluctuation rate of the dynamic magnetic fields. The static case is approached when this ratio is $\ll 1$, whereas the fast fluctuation limit is approached when the ratio $\gg 1$.[23]

Following the same procedure described in Ref. [23], we can estimate the molecular spin correlation time, τ, of $[DyPyNO]_2$. At low temperatures (< 30 K), $\tau = 2/(3\lambda)$,[36,38,42] while at high temperatures $\tau = \lambda\Delta_0^2/2$,[38,42] where $\Delta_0 = 62(4)$ MHz is the value of Δ at the limit $T \to 0$. The low temperature estimate for τ is reliable as it depends only on λ, but the high temperature estimate relies on the assumption that the size of magnetic moment of the molecule is temperature independent. This assumption is correct (below 300 K) for the $TbPc_2$ molecule due to the large energy difference between the ground state manifold, $\mathbf{J} = 6$, and the next state, $\mathbf{J} = 5$ which is of the order of a few hundreds K. However, we note that this is not very accurate for the case for $[DyPyNO]_2$. Nevertheless, we plot τ in $[DyPyNO]_2$ as a function of temperature in Fig. 4 in the whole temperature range.

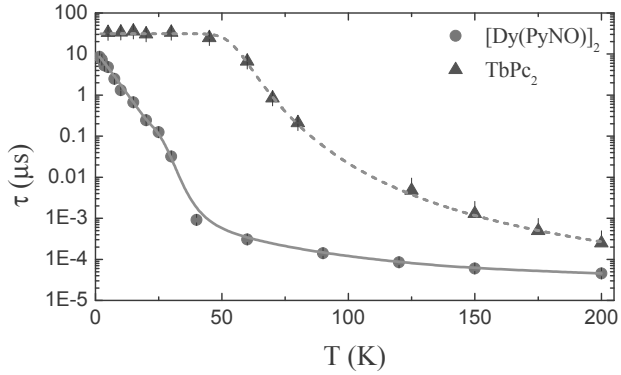

Figure 4: The correlation time for $[DyPyNO]_2$ (circles) and $TbPc_2$ (triangles) spin fluctuations as a function of temperature. The solid line is a guide to the eye and the dashed line is a fit as described in the text.

For comparison, we also plot the published results for bulk $TbPc_2$.[23] One can see clearly that even in the low temperature regime (< 30 K), there is a major difference between the temperature dependence observed in $TbPc_2$ compared to $[DyPyNO]_2$. While τ saturates

below $\sim$ 50 K in $TbPc_2$ (due to quantum tunneling), it remains strongly temperature dependent in $[DyPyNO]_2$. This is clear indication that even at $\sim$ 1.5 K, the relaxation of the magnetization in $[DyPyNO]_2$ is driven by thermally activated spin transitions. This could be a result of the weak antiferromagnetic coupling between the two Dy moments within each molecule, which becomes important at low T, splitting the ground state of the single ion. Therefore, thermally activated transitions among the split levels are possible at low T in the case of $[DyPyNO]_2$.

Below 20 K the average field distribution width is $\Delta = 72(5)$ mT. This can be calculated from dipolar field of Dy moments acting on the implanted muons. The distribution of static fields simply reflects the different stopping sites of the muons and various possible orientations of the Dy moments. *A priori*, we have no knowledge of the exact stopping site of the muon relative to the Dy ions. However, $[DyPyNO]_2$ has 36 fluorine atoms per molecule, whose high electron affinity provides a very attractive environment for positively charged muons.[43,44] Therefore, we assume that muons stop near the fluorine atoms. Two Dy spin configurations were considered in the calculation; (I) the Dy spins align along their easy axes and (II) they have no preferential direction. In both configurations we assume that the Dy magnetic moment corresponds to the ground state manifold, $J = 15/2$. Note, configuration (I) mimics $T \to 0$, where J_z can be either $\pm 15/2$ and thus we expect to get a maximum of 36 possible field values, corresponding to the 36 fluorine sites. In contrast, configuration (II) represent a slowly fluctuating Dy moments (though static on the time scale of μSR) which can point in any direction.

The width of distributions, Δ^i_{c1} for $i = x$, y and z in configuration (I) are $\sim$ 85, $\sim$ 123 and $\sim$ 104 mT, respectively. In configuration (II), the dipolar field distribution is almost Gaussian for all three components of the field (Fig. 5), with $\Delta^i_{c2} \sim 81$, ~ 97 and ~ 95 mT for the $i = x$, y and z components, respectively. These are to be compared to the isotropic $\Delta \sim 72$ mT obtained from the experiment. Note that Δ^i_{c1} is large and anisotropic, while Δ^i_{c2} is more isotropic and closer to the value obtained experimentally, as clearly seen in Fig. 5.

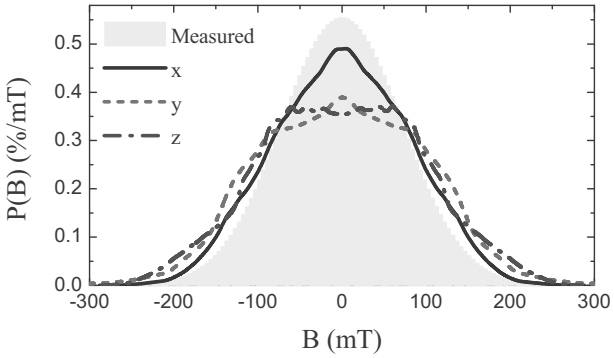

Figure 5: The calculated magnetic field distribution along each component at fluorine sites in the $[DyPyNO]_2$ molecule. The shaded area represents the isotropic distribution extracted from the measurements.

This result indicates that configuration (II) better reflects the experimental situation at low temperatures, *i.e.* the Dy moments can point in any direction. This is also consistent with our previous conclusion regarding the thermally activated nature of the spin fluctuations at low T. The somewhat larger calculated values of Δ compared to the experiment may be due to the assumption that the muon sites are identical to the fluorine sites, while in reality they are slightly farther from the Dy ions.

Conclusions

In conclusion, we find that the bulk static and dynamic magnetic properties of the $[DyPyNO]_2$ SMM are fully maintained in films. This is one of the few SMM examples that exhibit this robustness under sublimation and significant alteration of its environment. This is particularly relevant given that the packing of the molecules in the film is different from the bulk, thus proving that the detected spin dynamics is dominated by a pure SMM behavior. Stability of this molecular systems has been further confirmed by XPS and ToF-SIMS techniques validating the relevance of a multi-technique approach in the characterization of fragile molecular systems. Such robust behaviour is key for future developments since it allows engineering of SMM-based devices, where the magnetic properties of the SMM con-

stituents are predictable and controllable. We also find that the molecular spin fluctuations of $[DyPyNO]_2$ remain thermally activated down to ~ 1.5 K, reaching a value of $\tau \sim 8.5$ μs. At these temperatures, such fluctuations between the ground and excited spin states are suppressed due to the relatively large energy gap (~ 167 K) between them.[25] Therefore, we believe that these fluctuations are within the single ion ground state manifold, which is split due to the weak antiferromagnetic coupling between the two Dy spins. Finally, we point out that unlike other SMM films, such as $TbPc_2$, we detect no depth dependence of the spin correlation time in $[DyPyNO]_2$ films; not even near the surface or substrate interface.

Methods

Thin film samples were fabricated using a homemade molecular evaporator chamber, equipped with a quartz crucible. The crucible temperature was monitored using a type-K thermocouple inserted in the pressed powder sample. The molecular deposition rate was monitored using a quartz crystal microbalance (QCM). For the $[DyPyNO]_2$ thin-film evaporation, the temperature of the crucible was initially ramped slowly up to 380 K, where a reduction in the QCM oscillation frequency is detected accompanied by an increase in the chamber pressure from 1×10^{-7} to 1.5×10^{-6} mbar. At this temperature a deposition rate of 1.3 Å/s is deduced from the calibration of the QCM based on the density extracted from X-ray diffraction (XRD) analysis.[25] The system was maintained at this temperature for the duration of the film deposition. The molecular film used for the LE-μSR measurements was evaporated on top of a 100 nm thick gold film deposited by thermal evaporation on Muscovite mica. The thickness of the $[DyPyNO]_2$ and gold layers together was estimated using AFM scratching measurements (see SI).

In μSR measurements, 100% spin polarized muons are implanted into the sample and used as local probes to sense dipolar magnetic fields from neighbouring SMMs, thus providing a direct observation of their spin/magnetic moment and its temporal fluctuations. The

quantity of interest in these measurements is the muon spin polarization (along the initial spin direction, z) as a function of time, $P_z(t)$. The implantation energy of muons in conventional μSR is usually fixed at ~ 4 MeV, which corresponds to an implantation depth of the order of 100 microns in typical density materials. In contrast, the implantation energy (E) in LE-μSR experiments can be varied between 1 keV and 25 keV, which corresponds to implantation depths of 1 nm to 150 nm. This E tunability is the key feature that makes LE-μSR suitable for studies of thin film materials. The fitting of the muons spin polarization, $P_z(t)$, was performed using the musrfit program.[45]

Supporting Information Available

Full charecterization data and analysis of XPS, ToF-SIMS, AFM and XRD results as well as detailed depth dependence from LE-μSR measurements. This material is available free of charge *via* the Internet at `http://pubs.acs.org/`.

Acknowledgement

This work is based on experiments performed at the Swiss muon source SμS, Paul Scherrer Institute, Villigen, Switzerland. Part of this work has been supported by the ERC Advanced Grant MolNanoMaS (proj. n° 267746), and by Italian MIUR through PRIN "Record" (20097X44S7) and FIRB "NanoPlasMag" (RBFR10OAI0) projects. We thank S. Ciattini and L. Chelazzi for technical support with the XRD measurements. We would also like to thank R. F. Kiefl for fruitful discussions.

Conflict of Interest: The authors declare no competing financial interest.

References

1. Gatteschi, D.; Sessoli, R.; Villain, J. *Molecular Nanomagnets*; Oxford University Press, 2006.

2. Gómez-Coca, S.; Aravena, D.; Morales, R.; Ruiz, E. Large Magnetic Anisotropy in Mononuclear Metal Complexes. *Coord. Chem. Rev.* **2015**, *289-290*, 379–392.

3. Holmberg, R. J.; Murugesu, M. Adhering Magnetic Molecules to Surfaces. *J. Mater. Chem. C* **2015**, *3*, 11986–11998.

4. Caneschi, A.; Gatteschi, D.; Totti, F. Molecular Magnets and Surfaces: A Promising Marriage. A DFT Insight. *Coord. Chem. Rev.* **2015**, *289-290*, 357–378.

5. Cornia, A.; Mannini, M.; Sainctavit, P.; Sessoli, R. Chemical Strategies and Characterization Tools for the Organization of Single Molecule Magnets on Surfaces. *Chem. Soc. Rev.* **2011**, *40*, 3076–3091.

6. Mannini, M.; Pineider, F.; Sainctavit, P.; Danieli, C.; Otero, E.; Sciancalepore, C.; Talarico, A. M.; Arrio, M.; Cornia, A.; Gatteschi, D.; Sessoli, R. Magnetic Memory of a Single-Molecule Quantum Magnet Wired to a Gold Surface. *Nature Mater.* **2009**, *8*, 194–197.

7. Mannini, M.; Pineider, F.; Danieli, C.; Totti, F.; Sorace, L.; Sainctavit, P.; Arrio, M.; Otero, E.; Joly, L.; Cezar, J. C.; Cornia, A.; Sessoli, R. Quantum Tunnelling of the Magnetization in a Monolayer of Oriented Single-Molecule Magnets. *Nature* **2010**, *468*, 417–421.

8. Mannini, M.; Bertani, F.; Tudisco, C.; Malavolti, L.; Poggini, L.; Misztal, K.; Menozzi, D.; Motta, A.; Otero, E.; Ohresser, P.; Sainctavit, P.; Condorelli, G. G.; Dalcanale, E.; Sessoli, R. Magnetic Behaviour of $TbPc_2$ Single-Molecule Magnets Chemically Grafted on Silicon Surface. *Nat. Commun.* **2014**, *5*, 4582.

9. Katoh, K.; Yoshida, Y.; Yamashita, M.; Miyasaka, H.; Breedlove, B. K.; Kajiwara, T.; Takaishi, S.; Ishikawa, N.; Isshiki, H.; Zhang, Y. F.; Komeda, T.; Yamagishi, M.; Takeyaet, J. Direct Observation of Lanthanide(III)-Phthalocyanine Molecules

on Au(111) by Using Scanning Tunneling Microscopy and Scanning Tunneling Spectroscopy and Thin-Film Field-Effect Transistor Properties of Tb(III)- and Dy(III)-Phthalocyanine Molecules. *J. Am. Chem. Soc.* **2009**, *131*, 9967–9976.

10. Malavolti, L.; Lanzilotto, V.; Ninova, S.; Poggini, L.; Cimatti, I.; Cortigiani, B.; Margheriti, L.; Chiappe, D.; Otero, E.; Sainctavit, P.; Totti, F.; Cornia, A.; Mannini, M.; Sessoli, S. Magnetic Bistability in a Submonolayer of Sublimated Fe_4 Single-Molecule Magnets. *Nano Lett.* **2015**, *15*, 535–541.

11. Rigamonti, L.; Piccioli, M.; Malavolti, L.; Poggini, L.; Mannini, M.; Totti, F.; Cortigiani, B.; Magnani, A.; Sessoli, R.; Cornia, A. Enhanced Vapor-Phase Processing in Fluorinated Fe_4 Single-Molecule Magnets. *Inorg. Chem.* **2013**, *52*, 5897–5905.

12. Barra, A.; Caneschi, A.; Cornia, A.; Fabrizi de Biani, F.; Gatteschi, D.; Sangregorio, C.; Sessoli, R.; Sorace, L. Single-Molecule Magnet Behavior of a Tetranuclear Iron(III) Complex. The Origin of Slow Magnetic Relaxation in Iron(III) Clusters. *J. Am. Chem. Soc.* **1999**, *121*, 5302–5310.

13. Ishikawa, N.; Sugita, M.; Ishikawa, T.; Koshihara, S.-y.; Kaizu, Y. Lanthanide Double-Decker Complexes Functioning As Magnets at the Single-Molecular Level. *J. Am. Chem. Soc.* **2003**, *125*, 8694–8695.

14. Fu, Y.-S.; Schwï£¡bel, J.; Hla, S.-W.; Dilullo, A.; Hoffmann, G.; Klyatskaya, S.; Ruben, M.; Wiesendanger, R. Reversible Chiral Switching of Bis(phthalocyaninato) Terbium(III) on a Metal Surface. *Nano Lett.* **2012**, *12*, 3931–3935.

15. Luzon, J.; Sessoli, R. Lanthanides in Molecular Magnetism: So Fascinating, So Challenging. *Dalton Trans.* **2012**, *41*, 13556–13567.

16. Woodruff, D. N.; Winpenny, R. E. P.; Layfield, R. A. Lanthanide Single-Molecule Magnets. *Chem. Rev.* **2013**, *113*, 5110–5148.

17. Guo, Y.-N.; Xu, G.-F.; Wernsdorfer, W.; Ungur, L.; Guo, Y.; Tang, J.; Zhang, H.-J.; Chibotaru, L. F.; Powell, A. K. Strong Axiality and Ising Exchange Interaction Suppress Zero-Field Tunneling of Magnetization of an Asymmetric Dy_2 Single-Molecule Magnet. *J. Am. Chem. Soc.* **2011**, *133*, 11948–11951.

18. Zhang, P.; Zhang, L.; Tang, J. Lanthanide Single Molecule Magnets: Progress and Perspective. *Dalton Trans.* **2015**, *44*, 3923–3929.

19. Gregson, M.; Chilton, N. F.; Ariciu, A.-M.; Tuna, F.; Crowe, I.; Lewis, W.; Blake, A. J.; Collison, D.; McInnes, E. J. L.; Winpenny, R. E. P.; Liddle, S. T. A Monometallic Lanthanide Bis(methanediide) Single Molecule Magnet with a Large Energy Barrier and Complex Spin Relaxation Behaviour. *Chem. Sci.* **2015**, *7*, 155–165

20. Urdampilleta, M.; Klayatskaya, S.; Ruben, M.; Wernsdorfer, W. Magnetic Interaction Between a Radical Spin and a Single-Molecule Magnet in a Molecular Spin-Valve. *ACS Nano* **2015**, *9*, 4458–4464.

21. Thiele, S.; Balestro, F.; Ballou, R.; Klyatskaya, S.; Ruben, M.; Wernsdorfer, W. Electrically Driven Nuclear Spin Resonance in Single-Molecule Magnets. *Science* **2014**, *344*, 1135–1138.

22. Margheriti, L.; Chiappe, D.; Mannini, M.; Car, P.; Sainctavit, P.; Arrio, M.; de Mongeot, F. B.; Cezar, J. C.; Piras, F. M.; Magnani, A.; Otero, E.; Caneschi, A.; Sessoli, R. X-Ray Detected Magnetic Hysteresis of Thermally Evaporated Terbium Double-Decker Oriented Films. *Adv. Mater.* **2010**, *22*, 5488–5493.

23. Hofmann, A.; Salman, Z.; Mannini, M.; Amato, A.; Malavolti, L.; Morenzoni, E.; Prokscha, T.; Sessoli, R.; Suter, A. Depth-Dependent Spin Dynamics in Thin Films of TbPc2 Nanomagnets Explored by Low-Energy Implanted Muons. *ACS Nano* **2012**, *6*, 8390–8396.

24. Malavolti, L.; Mannini, M.; Car, P.-E.; Campo, G.; Pineider, F.; Sessoli, R. Erratic Magnetic Hysteresis of TbPc2 Molecular Nanomagnets. *J. Mater. Chem. C* **2013**, *1*, 2935–2942

25. Yi, X.; Bernot, K.; Pointillart, F.; Poneti, G.; Calvez, G.; Daiguebonne, C.; Guillou, O.; Sessoli, R. A Luminescent and Sublimable DyIII-Based Single-Molecule Magnet. *Chem. Eur. J.* **2012**, *18*, 11379–11387.

26. Yaouanc, A.; de Réotier, P. D. *Muon Spin Rotation, Relaxation, and Resonance: Applications to Condensed Matter*; OUP Oxford, 2010.

27. Prokscha, T.; Morenzoni, E.; Deiters, K.; Foroughi, F.; George, D.; Kobler, R.; Suter, A.; Vrankovic, V. The New μE4 Beam at PSI: A Hybrid-Type Large Acceptance Channel for the Generation of a High Intensity Surface-Muon Beam. *Nucl. Instrum. Meth. A* **2008**, *595*, 317–331.

28. Morenzoni, E.; Prokscha, T.; Suter, A.; Luetkens, H.; Khasanov, R. Nano-Scale Thin Film Investigations with Slow Polarized Muons. *J. Phys.: Condens. Matter* **2004**, *16*, S4583–S4601.

29. Salman, Z.; Chow, K. H.; Miller, R. I.; Morello, A.; Parolin, T. J.; Hossain, M. D.; Keeler, T. A.; MacFarlane, W. A.; Saadaoui, H.; Wang, D.; Sessoli, R.; Condorelli, G. G.; Kiefl, R. F. Local Magnetic Properties of a Monolayer of Mn_{12} Single Molecule Magnets. *Nano Lett.* **2007**, *7*, 1551.

30. Munery, S.; Ratel-Ramond, N.; Benjalal, Y.; Vernisse, L.; Guillermet, O.; Bouju, X.; Coratger, R.; Bonvoisin, J. Synthesis and Characterization of a Series of Ruthenium Tris(β-diketonato) Complexes by an UHV-STM Investigation and Numerical Calculations. *Eur. J. Inorg. Chem.* **2011**, *2011*, 2698–2705.

31. Cimatti, I.; Ninova, S.; Lanzilotto, V.; Malavolti, L.; Rigamonti, L.; Cortigiani, B.; Mannini, M.; Magnano, E.; Bondino, F.; Totti, F.; Cornia, A.; Sessoli, R. UHV Deposi-

tion and Characterization of a Mononuclear Iron(III) β-diketonate Complex on Au(111). *Beilstein J. Nanotechnol.* **2014**, *5*, 2139–2148.

32. Milanov, A. P.; Seidel, R. W.; Barreca, D.; Gasparotto, A.; Winter, M.; Feydt, J.; Irsen, S.; Becker, H.-W.; Devi, A. Malonate Complexes of Dysprosium: Synthesis, Characterization and Application for LI-MOCVD of Dysprosium Containing Thin Films. *Dalton Trans.* **2011**, *40*, 62–78.

33. Barreca, D.; Gasparotto, A.; Milanov, A.; Tondello, E.; Devi, A.; Fischer, R. A. Nanostructured Dy_2O_3 Films: An XPS Investigation. *Surf. Sci. Spectra* **2007**, *14*, 52–59.

34. Mazalov, L.; Trubina, S.; Kryuchkova, N.; Tarasenko, O.; Trubin, S.; Zharkova, G. X-Ray Photoelectron Study of Electron Density Distribution in Palladium(II) β-diketonate Complexes. *J. Struct. Chem.* **2007**, *48*, 253–261.

35. Popovici, D.; Czeremuzkin, G.; Meunier, M.; Sacher, E. Laser-Induced Metal-Organic Chemical Vapor Deposition (MOCVD) of Cu(hfac)(TMVS) on Amorphous Teflon AF1600: an XPS Study of the Interface. *Appl. Surf. Sci.* **1998**, *126*, 198–204.

36. Salman, Z.; Giblin, S. R.; Lan, Y.; Powell, A. K.; Scheuermann, R.; Tingle, R.; Sessoli, R. Probing the Magnetic Ground State of the Molecular Dysprosium Triangle with Muon Spin Relaxation. *Phys. Rev. B* **2010**, *82*, 174427.

37. Lord, J. S. Muon Methods for Studying Nanomagnetism. *J. Phys.: Conf. Ser.* **2005**, *17*, 81.

38. Uemura, Y. J.; Yamazaki, T.; Harshman, D. R.; Senba, M.; Ansaldo, E. J. Muon-Spin Relaxation in AuFe and CuMn Spin Glasses. *Phys. Rev. B* **1985**, *31*, 546–563.

39. Salman, Z.; Keren, A.; Mendels, P.; Marvaud, V.; Scuiller, A.; Verdaguer, M.; Lord, J. S.; Baines, C. Dynamics at $T \rightarrow 0$ in the Half-Integer Isotropic High Spin Molecules. *Phys. Rev. B* **2002**, *65*, 132403.

40. Branzoli, F.; Filibian, M.; Carretta, P.; Klyatskaya, S.; Ruben, M. Spin Dynamics in the Neutral Rare-Earth Single-Molecule Magnets $[TbPc_2]^0$ and $[DyPc_2]^0$ from μSR and NMR Spectroscopies. *Phys. Rev. B* **2009**, *79*, 220404.

41. Branzoli, F.; Carretta, P.; Filibian, M.; Graf, M. J.; Klyatskaya, S.; Ruben, M.; Coneri, F.; Dhakal, P. Spin and Charge Dynamics in $[TbPc_2]^0$ and $[DyPc_2]^0$ Single-Molecule Magnets. *Phys. Rev. B* **2010**, *82*, 134401.

42. Hayano, R. S.; Uemura, Y. J.; Imazato, J.; Nishida, N.; Yamazaki, T.; Kubo, R. Zero-and Low-Field Spin Relaxation Studied by Positive Muons. *Phys. Rev. B* **1979**, *20*, 850–859.

43. Brewer, J. H.; Kreitzman, S. R.; Noakes, D. R.; Ansaldo, E. J.; Harshman, D. R.; Keitel, R. Observation of Muon-Fluorine "Hydrogen Bonding" in Ionic Crystals. *Phys. Rev B* **1986**, *33*, 7813–7816.

44. Lancaster, T.; Blundell, S. J.; Baker, P. J.; Brooks, M. L.; Hayes, W.; Pratt, F. L.; Manson, J. L.; Conner, M. M.; Schlueter, J. A. Muon-Fluorine Entangled States in Molecular Magnets. *Phys. Rev. Lett.* **2007**, *99*, 267601.

45. Suter, A.; Wojek, B. M. Musrfit: A Free Platform-Independent Framework for μSR Data Analysis. *Physics Procedia* **2012**, *30*, 69–73.

Graphical TOC Entry